Acta Pharmacologica Sinica

www.nature.com/aps

ARTICLE

Colon-targeted S100A8/A9-specific peptide systems ameliorate colitis and colitis-associated colorectal cancer in mouse models

Euni Cho[1,2], Seok-Jun Mun[1,2], Hyo Keun Kim[2,3], Yu Seong Ham[2,3], Woo Jin Gil[2,3] and Chul-Su Yang[2,3,4]✉

The link between chronic inflammation and cancer development is well acknowledged. Inflammatory bowel disease including ulcerative colitis and Crohn's disease frequently promotes colon cancer development. Thus, control of intestinal inflammation is a therapeutic strategy to prevent and manage colitis-associated colorectal cancer (CRC). Recently, gut mucosal damage-associated molecular patterns S100A8 and S100A9, acting via interactions with their pattern recognition receptors (PRRs), especially TLR4 and RAGE, have emerged as key players in the pathogenesis of colonic inflammation. We found elevated serum levels of S100A8 and S100A9 in both colitis and colitis-associated CRC mouse models along with significant increases in their binding with PRR, TLR4, and RAGE. In this study we developed a dual PRR-inhibiting peptide system (rCT-S100A8/A9) that consisted of TLR4- and RAGE-inhibiting motifs derived from S100A8 and S100A9, and conjugated with a CT peptide (TWYKIAFQRNRK) for colon-specific delivery. In human monocyte THP-1 and mouse BMDMs, S100A8/A9-derived peptide comprising TLR4- and RAGE-interacting motif (0.01, 0.1, 1 μM) dose-dependently inhibited the binding of S100 to TLR4 or RAGE, and effectively inhibited NLRP3 inflammasome activation. We demonstrated that rCT-S100A8/A9 had appropriate drug-like properties including in vitro stabilities and PK properties as well as pharmacological activities. In mouse models of DSS-induced acute and chronic colitis, injection of rCT-S100A8/A9 (50 μg·kg^{-1}·d^{-1}, i.p. for certain consecutive days) significantly increased the survival rates and alleviated the pathological injuries of the colon. In AOM/DSS-induced colitis-associated colorectal cancer (CAC) mouse model, injection of rCT-S100A8/A9 (50 μg·kg^{-1}·d^{-1}, i.p.) increased the body weight, decreased tumor burden in the distal colon, and significantly alleviated histological colonic damage. In mice bearing oxaliplatin-resistant CRC xenografts, injection of rCT-S100A8/A9 (20 μg/kg, i.p., every 3 days for 24–30 days) significantly inhibited the tumor growth with reduced EMT-associated markers in tumor tissues. Our results demonstrate that targeting the S100-PRR axis improves colonic inflammation and thus highlight this axis as a potential therapeutic target for colitis and CRC.

Keywords: colitis; colorectal cancer; S100A8/A9; TLR4; RAGE; NLRP3 inflammasome

Acta Pharmacologica Sinica (2024) 45:581–593; https://doi.org/10.1038/s41401-023-01188-2

INTRODUCTION

Inflammatory bowel disease (IBD), such as ulcerative colitis and Crohn's disease, is a chronic, immune-mediated inflammatory disease of the intestinal tract [1]. It is characterized by prolonged intestinal inflammation, which causes intractable ulcers to form and results in serious destruction of the intestinal mucosa [2]. Although the pathophysiology underlying IBD is not fully understood, deregulated cytokines and immune cells as well as intestinal dysbiosis have been shown to be associated with the persistent inflammation. Patients with IBD have a higher risk of developing colitis-associated colorectal cancer (CRC) [3], with an incidence rate of 15%–20% [4], underscoring the significance of the association between chronic inflammation and cancer development.

To date, the most successful strategy for treating IBD has been the use of biological agents that specifically target the excessive activity of the adaptive immune system. A representative agent of this type is infliximab, a monoclonal antibody designed to inhibit tumor necrosis factor alpha (TNFα) [5]. Nevertheless, research has shown that a failure to respond to anti-TNFα therapy occurs in more than one-third of IBD patients [6]. There is thus an urgent need to develop a novel therapeutic approach for IBD. Meanwhile, current therapeutic strategies employed for the treatment of CRC involve the administration of chemotherapeutic agents (e.g., 5-fluorouracil, irinotecan, and oxaliplatin) and/or targeted therapies (e.g., cetuximab and bevacizumab) [7, 8]. In cases of late-stage and advanced metastatic disease, radiation therapy may be included as an optional component [9]. However, upon the prolonged use of these therapeutic strategies, resistance eventually develops in all CRC cells [10]. With the ongoing increases in the incidences of IBD and CRC globally, there is a pressing need for more effective therapeutic approaches that can effectively address the challenges of tolerance and immunogenicity.

S100A8 and S100A9 act as alarmins and play roles as danger-associated molecular patterns (DAMPs), which activate innate immune cascades via binding to pattern recognition receptors

[1]Department of Bionano Engineering, Hanyang University, Seoul 04673, Republic of Korea; [2]Center for Bionano Intelligence Education and Research, Ansan 15588, Republic of Korea; [3]Department of Molecular and Life Science, Hanyang University, Ansan 15588, Republic of Korea and [4]Department of Medicinal and Life Science, Hanyang University, Ansan 15588, Republic of Korea
Correspondence: Chul-Su Yang (chulsuyang@hanyang.ac.kr)
These authors contributed equally: Euni Cho, Seok-Jun Mun.

Received: 29 June 2023 Accepted: 29 October 2023
Published online: 1 December 2023

(PRRs), such as receptor for advanced glycation end products (RAGE) and toll-like receptor 4 (TLR4). This is turn results in the activation of downstream transcription factors such as nuclear factor-κB and the production of proinflammatory cytokines [11, 12]. Many studies have demonstrated elevated serum levels of S100A8/A9 in numerous inflammatory diseases including IBD, rheumatoid arthritis, psoriasis, and vasculitis [13–16]. S100A8 and S100A9 are also known to disrupt homeostasis of the intestinal mucosa and accelerate the progression of colitis by triggering a proinflammatory signaling cascade [17]. DAMPs also form a microenvironment that promotes the development of CRC, presumably by contributing to uncontrolled inflammatory responses [15]. Namely, chronic inflammation, initiated, perpetuated, and amplified by the S100A8/A9-PRRs axis, has been shown to be involved in the link between inflammation and cancer (colitis-CRC). Thus, to treat IBD and CRC, it may be therapeutically useful for treating IBD and CRC with therapeutic targeting potential.

Colon-specific drug delivery, which enables targeted drug delivery into the colon, holds significant promise for the localized treatment of various bowel diseases including ulcerative colitis, Crohn's disease, and colonic cancer [18]. Furthermore, in the context of IBD, implementing topical blockade specifically at the intestinal mucosa could be a promising therapeutic strategy with enhanced drug efficacy and reduced drug toxicity [19]. One study showed that inflamed colon could be targeted by a 12-residue peptide (TWYKIAFQRNRK) [20]. Encouraged by this, we previously developed a colon-specific delivery system with the ability to modulate NLRP3 inflammasome, which successfully targeted the colon [21].

Against this background, we hypothesized that a targeting strategy that involves using proinflammatory factors, S100A8 and S100A9, to block signaling mediated by two PRRs (TLR4 and RAGE) would be beneficial for IBD and CRC. Here, we developed a dual PRR-inhibiting peptide system that includes TLR4- and RAGE-inhibiting motifs derived from the sequences by which S100A8 and S100A9 interact with their PRRs. This system was further functionalized by the conjugation of a CT peptide for colon-specific delivery (rCT-S100A8/A9). This rCT-S100A8/A9 peptide system effectively inhibited TLR4- and RAGE-mediated signaling in various murine colitis models, including acute and chronic colitis induced by dextran sulfate sodium (DSS), as well as colorectal cancer induced by azoxymethane (AOM)/DSS. We also evaluated the potential application of rCT-S100A8/A9 in oxaliplatin-resistant colon cancer using xenograft models. The peptide system exhibited significant protective effects against all of these models. Our study presents a proof of concept for dual PRR-inhibiting systems as a means of preventing intestinal chronic inflammation, indicating their applicability for both IBD and CRC.

MATERIALS AND METHODS

Mice and cell culture

Wild-type C57BL/6 mice were purchased from Samtako Bio Korea (Gyeonggi-do, Republic of Korea). S100a8-KO (C57BL/6Smoc-*S100a8*^{em1Smoc}) and S100a9-KO (C57BL/6Smoc-*S100a9*^{em1Smoc}) mice were purchased from Shanghai Model Organisms Center, Inc. (Jinshan, China). Primary bone marrow-derived macrophages (BMDMs) were isolated from mice and cultured in DMEM for 3–5 days in the presence of M-CSF (416-ML; R&D Systems), as described previously [22]. HEK293T (ATCC-11268; American Type Culture Collection) in DMEM (GenDEPOT) or human monocytic THP-1 (ATCC-TIB-202) in RPMI1640 (GenDEPOT) containing 10% FBS (Gibco), sodium pyruvate, nonessential amino acids, penicillin G (100 IU/ml), and streptomycin (100 μg/ml).

To establish CRC cell models resistant to oxaliplatin, doxorubicin, or 5-FU, we exposed HT29, HT116, and SW480 cells to gradually increasing concentrations of oxaliplatin, doxorubicin, or 5-FU, as described previously [23–25]. The established oxaliplatin-, doxorubicin-, and 5-FU-resistant cells were named OxaR, DoxR, and 5-FuR cells, respectively.

Reagents and antibodies

LPS (*Escherichia coli* O111:B4, tlrl-eblps), adenosine 5′-triphosphate (ATP, tlrl-atpl), nigericin, monosodium urate crystals (MSU, tlrl-msu), poly(dA:dT) (tlrl-patc), and flagellin (FLA-ST, tlrl-stfla) were purchased from Invitrogen. Dextran sulfate sodium (DSS, 36–50 kDa) was purchased from MP Biomedicals.

Antibodies specific for NAMPT (ab236874) were purchased from Abcam. RAGE (RD9C2), TLR4 (25), Actin (I-19), ASC (N-15-R), IL-18 (H-173-Y), caspase-1 p10 (M-20), HA (12CA5), Flag (D-8), GST(B-14), Myc (9E10), and His (H-3) were purchased from Santa Cruz Biotechnology. Specific Abs against S100A8 (E4F8V), S100A9 (D3U8M), E-Cadherin (24E10), N-Cadherin (D4R1H), and β-Catenin (D10A8) were purchased from Cell Signaling Technology (Danvers, MA, USA). IL-1β (AF-401-NA) and NLRP3 (AG-20B-0014) were from R&D Systems and Adipogen, respectively.

Plasmid construction

HA or His-S100A8 or S100A9, Myc-TLR4, and Myc-RAGE plasmids were purchased from Addgene. Plasmids encoding different regions of S100A8 or S100A9 were generated by PCR amplification from full-length S100A8 or S100A9 cDNA and subcloning into a pEBG derivative encoding an N-terminal GST epitope tag between the *BamHI* and *NotI* sites. All constructs were sequenced to verify 100% correspondence with the original sequence.

Peptides

S100A8 or S100A9 peptides were commercially synthesized and purified in acetate salt form to avoid abnormal responses in cells by Peptron (Republic of Korea). The amino acid sequences of the peptides in this study are presented in Figs. 2a, b, and 3b. The endotoxin content, as measured by the *Limulus amebocyte* lysate assay (BioWhittaker), was less than 3–5 pg/ml at the concentrations of peptides used in the experiments.

Recombinant protein

To obtain recombinant rCT-S100A8/9 proteins (Fig. 4a), S100A8 or S100A9 amino acid (Figs. 2a, b, and 3b) and CT peptide (TWYKIAFQRNRK) colon-targeting sequences were cloned with an N-terminal 6×His tag into the pRSFDuet-1 Vector (Novagen). This was followed by expression induction, harvesting, and purification from the *Escherichia coli* expression strain BL21(DE3) pLysS, as described previously [22], in accordance with the standard protocols recommended by Novagen. rVehicle, rCT, or rCT-S100A8/9 was dialyzed with permeable cellulose membrane, tested for lipopolysaccharide contamination with a *Limulus amebocyte* lysate assay (BioWhittaker), and shown to contain <20 pg/ml lipopolysaccharide.

GST pulldown, immunoblot, and immunoprecipitation analyses

293T, BMDMs, and THP-1 cells were treated as indicated and processed for analysis by GST pulldown, Western blotting, and co-immunoprecipitation, as previously described [21, 26, 27]. For GST pulldown, 293T cells were harvested and lysed in NP-40 buffer supplemented with a complete protease inhibitor cocktail (Roche, Basel, Switzerland). After centrifugation, the supernatants were precleared with protein A/G beads at 4 °C for 2 h. Pre-cleared lysates were mixed with a 50% slurry of glutathione-conjugated Sepharose beads (Amersham Biosciences, Amersham, UK), and the binding reaction was incubated for 4 h at 4 °C. Precipitates were washed extensively with lysis buffer. Proteins bound to glutathione beads were eluted with sodium dodecyl sulfate (SDS) loading buffer by boiling for 5 min. For immunoprecipitation, cells were harvested and then lysed in NP-40 buffer supplemented with a complete protease inhibitor cocktail (Roche, Switzerland). After

pre-clearing with protein A/G agarose beads for 1 h at 4 °C, whole-cell lysates were used for immunoprecipitation with the indicated antibodies. Generally, 1–4 μg of commercial antibody was added to 1 ml of cell lysates and incubated at 4 °C for 8 to 12 h. After the addition of protein A/G agarose beads for 6 h, immunoprecipitates were extensively washed with lysis buffer and eluted with SDS loading buffer by boiling for 5 min. For immunoblotting (IB), polypeptides were resolved by SDS-polyacrylamide gel electrophoresis and transferred to a PVDF membrane (Bio-Rad, Hercules, CA, USA). Immunodetection was achieved with specific antibodies. Antibody binding was visualized by chemiluminescence (ECL; Millipore, Burlington, MA, USA) and detected using a Vilber chemiluminescence analyzer (Fusion SL 3; Vilber Lourmat).

Flow cytometry

S100A8 or S100A9 peptide or rCT-S100A8/9 was conjugated with Texas Red using the Texas Red® Conjugation Kit (Fast)-Lightning-Link (Abcam) to quantitatively measure the cellular uptake of macrophages and pharmacodynamics of the colitis model. The cells were thoroughly and quickly washed with pulse spin and immediately acquired for analyses in FACSCalibur (BD Biosciences, San Jose, CA, USA). The data were plotted using CellQuest software (BD Biosciences) and analyzed with FlowJo software (Tree Star, Ashland, OR, USA).

Enzyme-linked immunosorbent assay

Cell culture supernatants and mouse sera were analyzed for cytokine content using the BD OptEIA ELISA set (BD Pharmingen) for the detection of TNF-α, IL-6, IL-1β, and IL-18. All assays were performed as the manufacturer's recommendations.

Mouse models

DSS-induced acute or chronic colitis and AOM/DSS CRC mouse models were prepared using 6-week-old C57BL/6 female mice (Samtako, Osan, Republic of Korea), as previously described [21, 27]. To assess the induction of acute colitis, mice were exposed to 3% (*w/v*) dextran sodium sulfate (molecular weight: 36–50 kDa; MP Biomedicals, Santa Ana, CA, USA) dissolved in drinking water given *ad libitum*, as illustrated in Figs. 5a, e, and 6a. The DSS solutions were made freshly every 2 days. Control non-DSS-fed mice had access to sterile distilled water. The humane endpoint (euthanasia required) for body weight loss was 20% (compared with the original body weight of an animal). Body weight loss could not exceed 20% without an approved exception request.

Female athymic nude mice of 4–6 weeks of age (Central Lab. Animal, Seoul, Republic of Korea) were used for the tumor xenograft experiments, as previously described [23]. Animals were subcutaneously injected with 1×10^6 HCT116 cells suspended in 0.1 mL of cell medium into the right axillary region and observed for 7–10 days with the measurement of tumor volume. The treatment was initiated when the tumor size reached an average volume of 200 or 600 mm^3. The tumor volume was measured every third day with skin calipers and calculated as the tumor length × tumor $width^2 \times 0.5$ and represented in mm^3. All animals were maintained in a specific-pathogen-free environment. All animal-related procedures were reviewed and approved by the Institutional Animal Care and Use Committee of Hanyang University (protocol numbers 2022-0145 and 2022-0266).

Clinical score and histology

For the clinical score of colitis, body weight, occult or gross blood lost via the rectum, and stool consistency were determined every other day during the induction of colitis. The clinical score was assessed by two trained investigators blinded to the treatment [21, 27]. For immunohistochemical analysis of the tissue sections, mouse distal colon tissues were fixed in 10% formalin and embedded in paraffin. Paraffin sections (4 μm) were cut and stained with hematoxylin and eosin (H&E). Histopathological scoring was performed, in which a board-certified pathologist (Dr. Min-Kyung Kim, Kim Min-Kyung Pathology Clinic, Seoul, Korea) independently scored each organ section without prior knowledge of the treatment groups, as previously described [21, 23, 27].

Statistical analysis

All data were analyzed using Student's *t*-test with Bonferroni adjustment or ANOVA for multiple comparisons, and are presented as mean ± SD. Statistical analyses were conducted using the SPSS (Version 12.0) statistical software program (SPSS, Chicago, IL, USA). Differences were considered significant at $P < 0.05$. For survival, data were plotted for visual representation and analyzed by the product limit method of Kaplan and Meier, using the log-rank (Mantel-Cox) test for comparisons using GraphPad Prism (version 5.0; La Jolla, CA, USA).

RESULTS

Interactions between S100A8 or A9 and TLR4 or RAGE are elevated in colon lysates of mice with acute colitis, chronic colitis, and CRC

Under inflammatory stimuli, S100A8 and S100A9 are secreted at local sites of inflammation and interact with TLR4 or RAGE of immune cells, which amplifies inflammatory signaling cascades [28]. To confirm whether S100 proteins physically interact with TLR4 or RAGE, we performed a co-immunoprecipitation (co-IP) experiment under two conditions: Each tagged plasmid (Myc-TLR4 or RAGE, HA-S100A8, and His-S100A9) was co-expressed in HEK293T cells or recombinant S100A8 or S100A9 proteins (rHA-mS100A8 or rHis-mS100A9) were treated in BMDMs followed by co-immunoprecipitation with each cell lysate sample.

In HEK293T, co-IP assays demonstrated that both HA-S100A8 and His-S100A9 physically interacted with Myc-TLR4 or Myc-RAGE. In BMDMs, co-IP assays demonstrated that both rS100A8 and A9 physically interacted with endogenous TLR4 or RAGE, and interestingly rHis-mS100A9 showed stronger binding with PRRs (TLR4 and RAGE) than rHA-mS100A8 (Fig. 1a, b).

The physical interaction between S100 and PRRs is functionally relevant to their role in inflammatory responses [29]. Thus, we hypothesized that aberrant S100 expression may be associated with colon diseases such as IBD and CRC. To evaluate whether S100A8 and A9 are risk factors in IBD and CRC, we generated DSS-induced colitis models, including mouse models of acute colitis, chronic colitis, and CRC, as previously described [21]. We further analyzed S100A8 and A9 expression, and their physical interactions with PRRs in serum and colon lysates from mouse models of acute and chronic colitis and CRC. The levels of S100A8 and A9 proteins in serum were markedly increased, in the following order: acute colitis < chronic colitis < colorectal cancer mouse models. This suggested that the secretion of S100A8 and A9 was elevated in association with the level of inflammation, and in the case of CRC, it was found to be higher than in inflammatory disease (Fig. 1c). In addition, physical interactions between S100A8 or A9 and TLR4 or RAGE were observed in the colon lysates of each model, which were prominent in chronic colitis and CRC models, while intracellular expression levels of S100A8 and A9 were observed at similar levels among these models. Consistent with these findings, the physical interactions between S100A8 or A9 and TLR4 or RAGE were remarkably upregulated in mouse models of chronic colitis and CRC compared with the levels in acute colitis (Fig. 1d).

In line with these findings, the physical interactions of S100A8 and A9 with PRRs noticeably increased in association with increased disease severity in colon lysates of mouse models of acute colitis, chronic colitis, and even CRC. Taken together, the results suggest that the extracellular binding of S100A8 and S100A9 proteins to PRRs was elevated with chronic inflammation of the colon, which may contribute to the development of CRC.

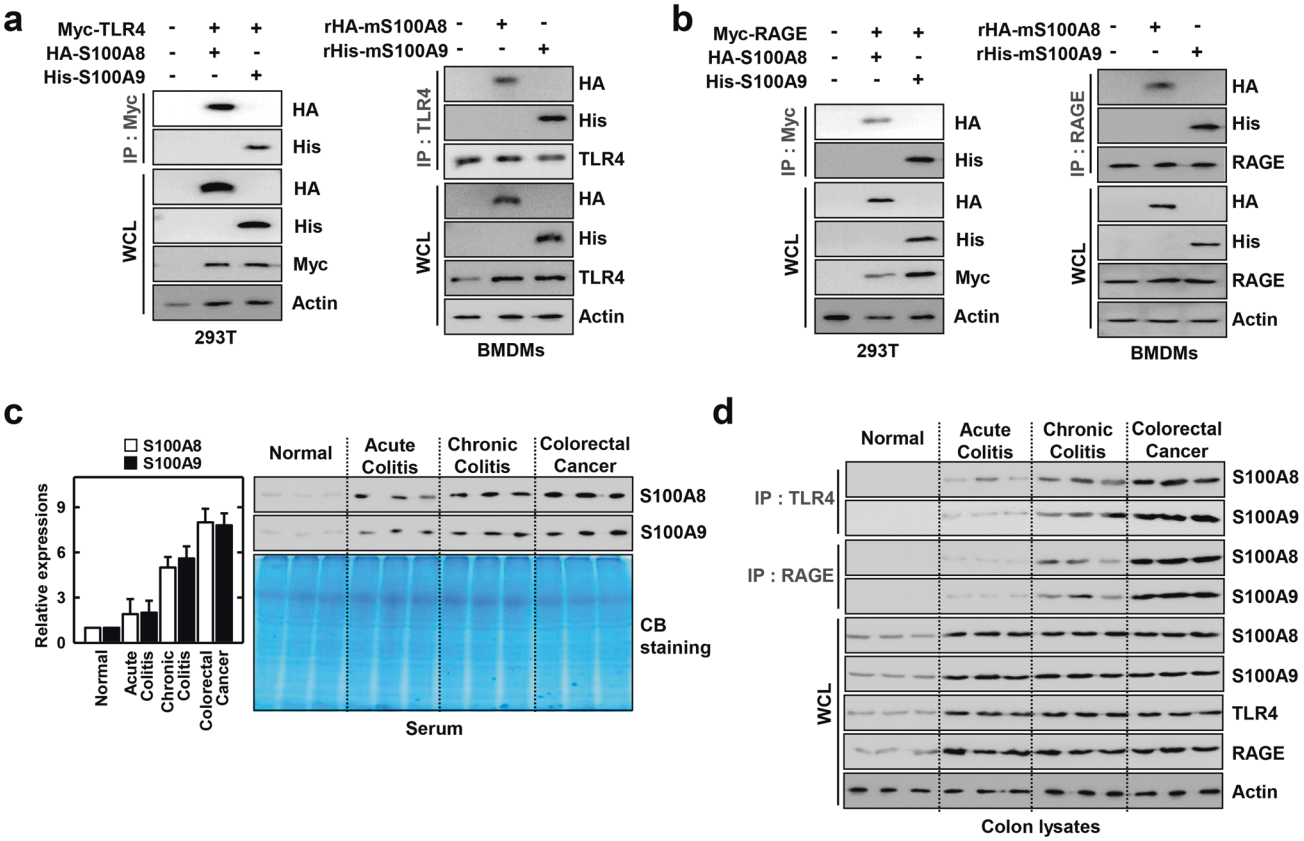

Fig. 1 Interaction between S100A8 or A9 and TLR4 or RAGE is increased in inflammation-related colon disease in mice. a, b 293T cells were transfected with Myc-TLR4 (**a**, left) or Myc-RAGE (**b**, left) and HA-S100A8 or His-S100A9. 293T cells were used for IP with αMyc, followed by IB with αHA or αHis. **a** Whole-cell lysates (WCLs) were used for IB with αHA, αHis, αMyc or αActin. BMDMs were incubated with rHA-S100A8 or rHis-S100A9 (5 μg/ml) for 10 min. BMDMs were subjected to IP with αTLR4 (**a**, right) or αRAGE (**b**, right), followed by IB with αHA, αHis, αTLR4 or αRAGE. WCLs were used for IB with αHA, αHis, αTLR4, αRAGE or αActin. **c** Left, Relative expression of S100A8 or S100A9 of normal, acute colitis, chronic colitis, and colorectal cancer in mouse. Biological replicates ($n = 10$) for each condition were performed. Right, Serum of normal, acute colitis, chronic colitis, and colorectal cancer of mouse were subjected to IB with αS100A8 or αS100A9. Coomassie (CB) stained gels show consistent loading of serum proteins. Data from three of ten samples are shown. **d** Colon lysates of normal, acute colitis, chronic colitis, and colorectal cancer of mouse were subjected to IP with αTLR4 or αRAGE, followed by IB with αS100A8 or αS100A9. WCLs were used for IB with αS100A8, αS100A9, αTLR4, αRAGE or αActin. The data are representative of seven independent experiments with similar results (**a**–**d**).

The presence of chronic inflammation caused by S100 protein exacerbates disease progression, suggesting an association between inflammation and cancer. Furthermore, this supports the association between high serum levels of S100A8/S100A9 and the clinical features of CRC patients [26].

S100A8/A9-derived peptides effectively block the interaction between TLR4 and RAGE

Both S100A8 and A9 contain two calcium-binding EF-hands (EF-hands I and II) with helix-loop-helix motifs linked by a hinge region and flanked by N- and C-terminal domains [30]. To identify the amino acid (aa) residues in each S100 protein that interact with TLR4 and RAGE, we constructed vectors that express truncated mutant S100A8 or A9 with GST tags. Each truncated mutant was designed by dividing the S100 protein sequence into 10-aa segments starting from the N-terminus. Each truncated mutant was then detected by GST pulldown assays in the presence of Myc-TLR4 or RAGE and subjected to immunoblotting assay. Domain mapping revealed that TLR4 interacts with S100A8 (aa 71–80) and S100A9 (aa 11–20), while RAGE was associated with S100A8 (aa 81–89) and S100A9 (aa 101–110) (Fig. 2a, b).

Using these potential TLR4- or RAGE-interacting motifs, we next synthesized an "S100A8 and S100A9 peptide" comprising the TLR4- and RAGE-interacting motifs of the S100A8 and S100A9 sequences, in which the aa sequence of the motif was selected based on the aa shared by mouse S100A8 and human S100A8, and mouse S100A9 and human S100A9, to adjust for the sequence differences between human and mouse (Fig. 2a, b, bottom).

Given the common binding site and the potential of the S100A8 (or S100A9) peptide to mimic the rHA-mS100A8 (or rHis-mS100A9) interaction with TLR4 or RAGE, we hypothesized that r-mS100A8 (or r-mS100A9) and S100A8 (or S100A9) peptide could compete for binding to TLR4 or RAGE. To test this hypothesis, we performed an in vitro binding assay with Texas Red-labeled rS100A8 (or A9) and unlabeled A8 (or A9) peptide in BMDMs by flow cytometry. The binding assay was performed by increasing the concentration of A8 or A9 peptide in the presence of Texas Red-labeled rS100A8 (or A9) to monitor the decrease in fluorescence resulting from the binding to TLR4 or RAGE. The results showed that target BMDMs exhibited clear decreases in fluorescent intensity upon increasing concentrations of A8 (or A9) peptide (Fig. S1). Interestingly, S100A9 peptide exhibited stronger inhibitory effects than A8 peptide. Furthermore, we performed a co-IP analysis between rHA-mS100A8 (or rHis-mS100A9) and TLR4 or RAGE with the increasing concentrations of S100A8 (or A9) peptide. Consistent with the fluorescent binding assay results, increasing amounts of S100A8 (or A9) peptide resulted in inhibition of the rS100A8 (or A9)-TLR4 (or RAGE) interaction (Fig. 2c). This demonstrated that

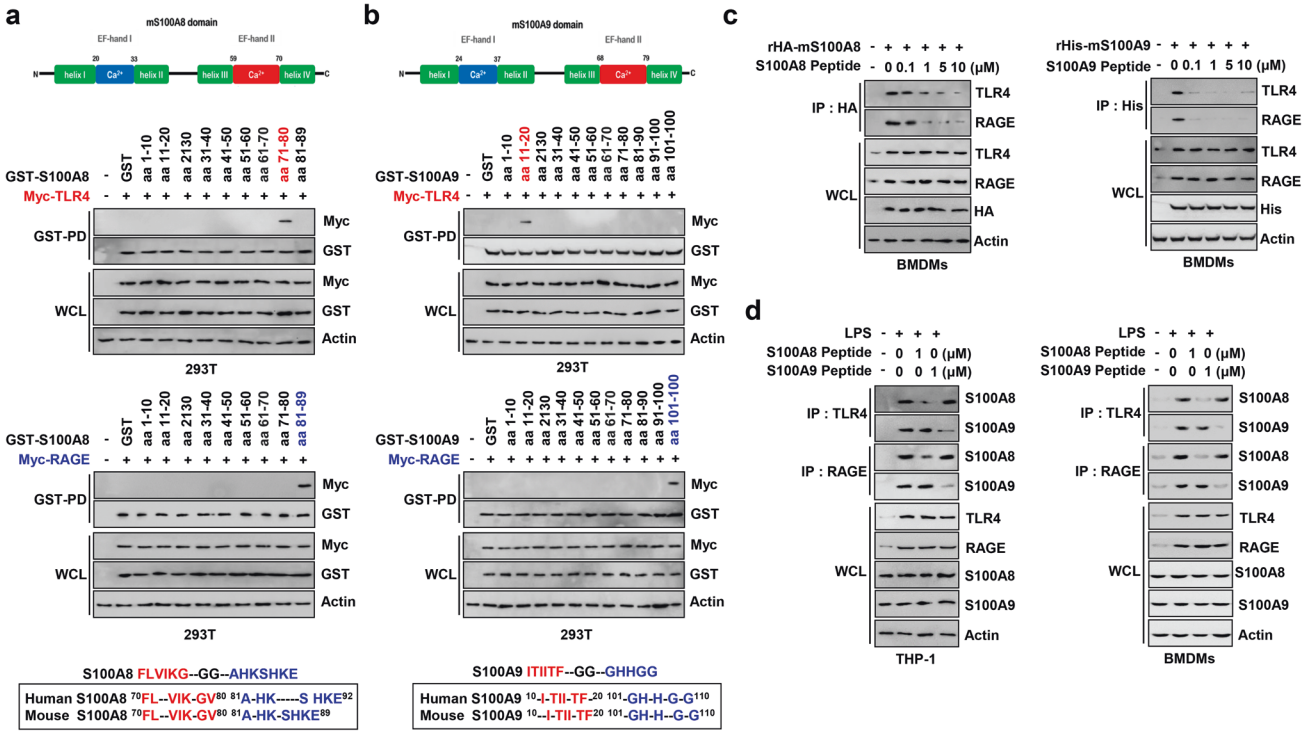

Fig. 2 Discovery and design of S100A8/A9 peptides that inhibit essential regions binding to TLR4 and RAGE. a, **b** Schematic diagram of the structures of S100A8 (**a**) and S100A9 (**b**) (upper). 293 T cells were transfected with GST-S100A8 (left), S100A9 (right) or its mutants, and Myc-TLR4 or Myc-RAGE. 293 T cells were subjected to GST pulldown, followed by IB with αMyc or αGST. WCLs were used for IB with αMyc, αGST or αActin. Bottom, Peptide design of S100A8 and S100A9 comprising TLR4 and RAGE-interacting motifs of S100A8 and S100A9 sequence in which a sequence of the motif was selected by shared aa between human and mouse. **c** BMDMs were incubated with rHA-S100A8 or rHis-S100A9 (5 μg/ml) for 10 min, in presence of S100A8 or S100A9 peptide for 1 h. BMDMs were subjected to IP with αHA or αHis, followed by IB with αTLR4 or αRAGE. WCLs were used for IB with αHA, αHis, αTLR4, αRAGE or αActin. **d** THP-1 or BMDMs were stimulated with LPS (100 ng/ml) for 18 h, in presence of S100A8 or S100A9 peptide for 1 h. BMDMs were subjected to IP with αTLR4 or αRAGE, followed by IB with αS100A8 or αS100A9. WCLs were used for IB with αTLR4, αRAGE, αS100A8, αS100A9 or αActin. The data are representative of seven independent experiments with similar results (**a**–**d**).

S100A8 (or A9) peptide can outcompete full-length S100A8 (or A9) for binding to TLR4 or RAGE.

We next assessed whether A8 (or A9) peptide might block the endogenous binding of S100A8 (or A9) with TLR4 or RAGE in phagocytes. LPS treatment with immune cells increased the expression of PRRs, such as TLR4 and RAGE, as well as the secretion of S100 proteins [31]; thus experiments were conducted under LPS treatment conditions. Specifically, we exposed LPS-treated THP-1 or BMDMs to A8 or A9 peptides, followed by co-IP with TLR4 or RAGE (Fig. 2d). The results showed that S100A8 (or A9)-TLR4 (or RAGE) interactions were increased in LPS-primed phagocytes (THP-1 and BMDMs), while their intracellular expression levels were unchanged. Notably, the endogenous binding of S100 with the receptors were observed to be inhibited in both LPS-primed THP-1 and BMDMs upon A8 (or A9) peptide treatment (Fig. 2d). Furthermore, the interactions of S100-receptor co-precipitated specifically in human monocyte THP-1 and mouse BMDMs, indicating that the inhibitory effects of the peptides are conserved in both humans and mice.

Taking the obtained findings together, A8 or A9 peptide comprising TLR4- and RAGE-interacting motif can successfully inhibit the binding of S100 to TLR4 or RAGE. These findings suggest the potential of peptides derived from S100 proteins to regulate inflammation.

S100A8/A9 peptide inhibits activation of the NLRP3 inflammasome

The NLRP3 inflammasome, a subset of cytosolic protein complexes, plays a crucial role in sensing pathogens and initiating inflammatory responses under both physiological and pathological conditions. Dysregulated activation of the NLRP3 inflammasome has been implicated in the development of IBD [32, 33].

To investigate the role of S100A8 (or S100A9) in activating the NLRP3 inflammasome, we examined whether the interaction of S100A8 (or S100A9) with TLR4 or RAGE was involved in NLRP3 inflammasome activation. We found that S100A8 (or S100A9) expressed by an NLRP3 inflammasome inducer (LPS/ATP) increased extracellular S100 secretion and markedly increased the interaction of S100 with TLR4 and RAGE in both THP-1 and BMDMs. We also found that these interactions were successfully inhibited by A8 or A9 peptide (Fig. 3a).

To improve the potency of the peptides, we next designed multifaceted S100A8/A9 peptide comprising (combining) the polypeptides of S100A8 or A9-derived TLR4-inhibited motifs (FLVIKG-GG-ITIITF) and RAGE-inhibited motifs (AHKSHK-GG-GHHGG) (Fig. 3b upper). In LPS-primed phagocytes treated with ATP, the S100A8/A9 peptide showed higher inhibitory activity on the extracellular binding of S100-TLR4/RAGE interactions than A8 or A9 peptide alone (Fig. 3b). From the biological testing, the S100A8/A9 peptide as a dual TLR4/RAGE inhibitor was tested in vitro at a concentration of 0.1 μM.

To assess the effect of S100A8/A9 peptide on the activation of NLRP3 inflammasome, we next investigated NLPR3-ASC complex formation, caspase-1 activation, IL-1β, and IL-18 production, and the maturation and secretion of pro-caspase-1 and pro-IL-1β/IL-18, which play crucial roles in inflammasome activation and the pathogenesis of IBD [34].

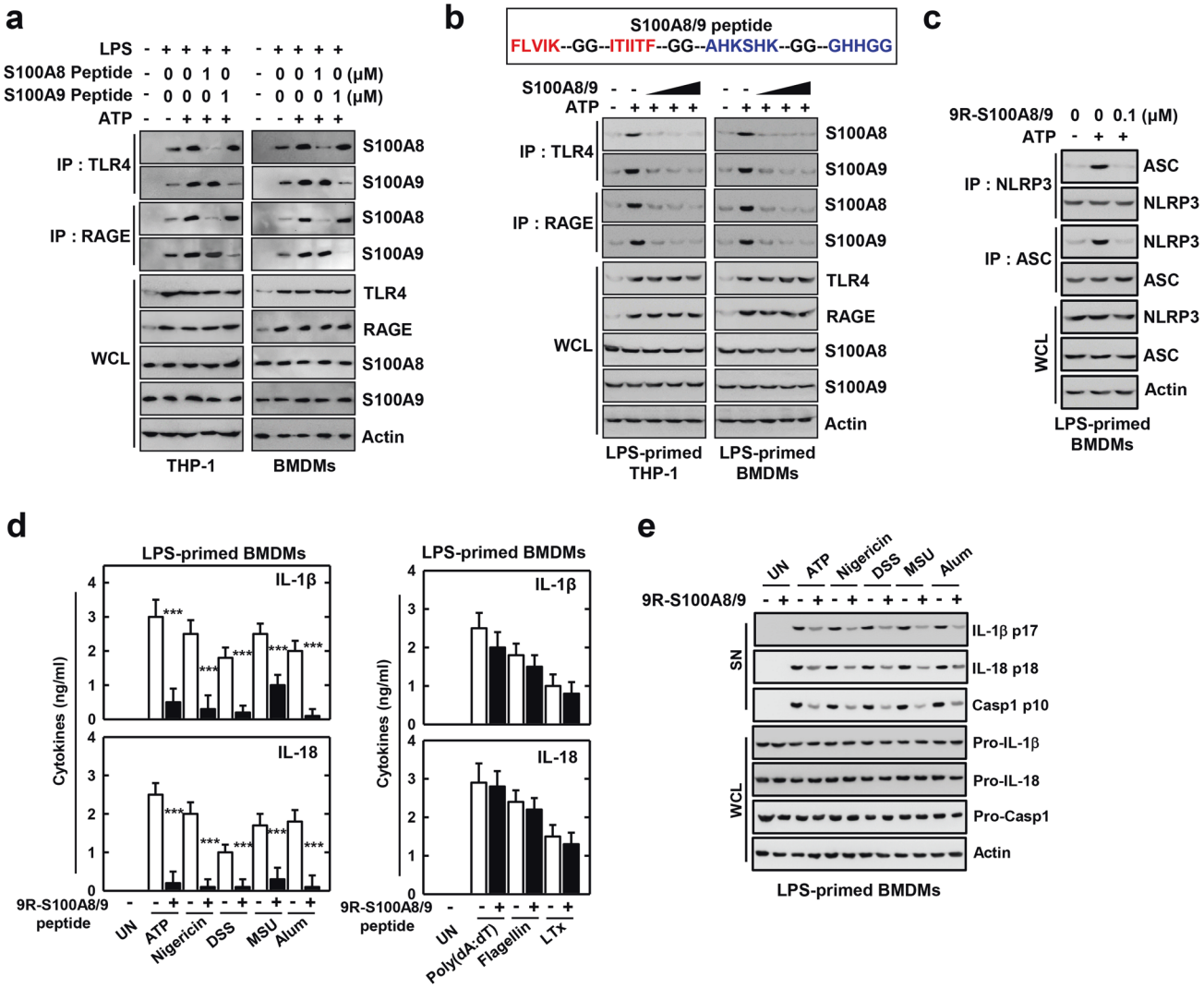

Fig. 3 S100A8/A9 peptide inhibits the activation of NLRP3 inflammasome. a LPS-primed THP-1 or BMDMs were treated with S100A8 or S100A9 peptide for 1 h, and then activated with ATP (1 mM) for 30 min, followed by IP with αTLR4 or αRAGE, followed by IB with αS100A8 or αS100A9. WCLs were used for IB with αTLR4, αRAGE, αS100A8, αS100A9 or αActin. **b** Schematic in design of S100A8/9 peptide (upper). LPS-primed THP-1 or BMDMs were treated with S100A8/9 peptide (0.01, 0.1, 1 μM) for 1 h, and then activated with ATP for 30 min The experimental conditions follow the same pattern as outlined in (**a**). **c** BMDMs were subjected to IP with αNLRP3 or αASC, followed by IB with αASC or αNLRP3. WCLs were used for IB with αNLRP3, αASC or αActin. **d**, **e** LPS-primed BMDMs were treated with 9R-S100A8/9 peptide (0.1 μM) for 1 h and stimulated with ATP, nigericin, MSU, Alum, poly (dA:dT), Flagellin or LTx for 1 h or DSS for 18 h. **d** ELISA for IL-1β and IL-18. **e** IB in supernatant (SN) with αIL-1β p17, αIL-18 p18 or αCasp1 p10 and WCL with αPro-IL-1β, αPro-IL-18, αPro-Casp1, or αActin. Data shown are the means ± SD of four experiments (**d**). Statistical significance was determined by Student's *t*-test with Bonferroni adjustment (***$P < 0.001$) compared with untreated peptide (**d**). The data are representative of seven independent experiments with similar results (**a**–**c** and **e**).

As shown in Fig. 3c, co-IP assay revealed that 0.1 μM 9R-S100A8/A9 peptide successfully inhibited the NLPR3-ASC interactions in LPS-primed BMDMs stimulated with ATP. To further investigate whether S100A8/A9 peptide was associated with various NLRP3 inflammasome activators, including ATP, nigericin, DSS, monosodium urate crystals (MSU), and aluminum (Alum), and other inflammasomes, namely, the AIM2 [activated with poly(dA:dT)], NLRC4 (activated with *Salmonella* flagellin), and NLRP1 (activated with anthrax lethal toxin) inflammasomes [28], we treated LPS-primed BMDMs with S100A8/A9 peptide and various inflammasome stimuli. Although treatment with S100A8/A9 peptide significantly decreased the secretion levels of IL-1β and IL-18 in response to NLRP3 activators, they did not affect the levels of AIM2, NLRC4, or NLRP1 activators in LPS-primed BMDMs (Fig. 3d), indicating that 9R-S100A8/A9 peptide specifically regulates NLRP3 inflammasome activation. Moreover, the treatment of 9R-S100A8/A9 peptide significantly decreased the production of caspase-1, IL-1β, and IL-18 in response to various NLRP3 inflammasome activators, in LPS-primed BMDMs, whereas the levels of pro-IL-1β, pro-IL-18, and pro-Casp-1, derived from the priming steps of NLRP3 inflammasome, were unchanged (Fig. 3e). This suggested that S100A8/A9 peptide may be involved in the activation step of NLRP3 inflammasome activation, not the priming step.

In conclusion, these results indicate that S100A8/A9 peptides possess the ability to inhibit the binding of S100A8 or S100A9 to TLR4 and RAGE, thereby exerting potential in regulating the NLRP3 inflammasome pathway. Consequently, these findings suggest that S100A8/A9 peptides may hold therapeutic potential for treating chronic inflammatory conditions, including IBD.

In vitro stability, pharmacokinetics, and target to inflamed colon of rCT-S100A8/A9

According to the results presented above, A8/A9 peptide directly blocks the binding of S100A8 or A9 to extracellular TLR4 and RAGE

a

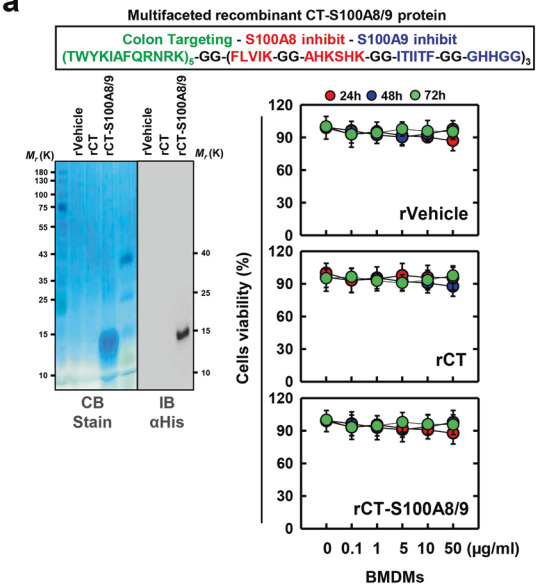

b

The results of *in vitro* plasma stability, microsomal stability, CYP inhibition and PK profile of S100A8/A9 peptides and rCT-S100A8/A9 proteins

	Stability (% remaining after 30 min)			CYP (% of control activity @ 10 μM)				
	PBS	Plasma	HLM	3A4	2D6	2C19	2C9	1A2
S100A8/A9	>100	>100	67.0	89.7	>100	99.2	93.1	79.8
rCT-S100A8/A9	>100	>100	92.1	85.8	>100	92.6	89.2	79.3

	PK parameters (ip, 1 mg/kg, mice (n = 5))[a]			
	T_{max} (h)	C_{max} (ng/mL)	AUC_{last} (ng·h/mL)	$T_{1/2}$ (h)
S100A8/A9	0.08 ± 0.0	102.14 ± 41.18	123.11 ± 29.17	0.42 ± 0.51
rCT-S100A8/A9	0.23 ± 0.0	213.12 ± 25.38	235.82 ± 51.48	1.91 ± 0.42

Fig. 4 The effects drug-like properties of rCT-S100A8/A9. a Schematic in design of rCT-S100A8/9(upper). Bacterially purified 6×His-rCT-S100A8/9, rVehicle or rCT were analyzed by Coomassie Blue staining or IB with αHis (lower, left). BMDMs were incubated with rVehicle, rCT or rCT-S100A8/9 for the indicated times and concentrations, then cell viability was measured with MTT assay (lower, right). **b** The results of in vitro plasma stability, microsomal stability, CYP inhibition, and PK profile of S100A8/A9 peptides and rCT-S100A8/A9 proteins. HLM human liver microsomes, CYP Cytochrome P450. [a]T_{max}, time to reach; AUC_{last}, total area under the plasma concentration−time curve from time zero to last measured time; C_{max}, peak plasma concentration.

and simultaneously attenuates the activation of NLRP3 inflammasome, suggesting the potential role of A8/A9 peptide in regulating inflammation in colitis. Thus, we further investigated whether this peptide has a protective effect on DSS-induced acute and chronic colitis models.

First, we constructed a multifaceted recombinant CT-S100A8/A9 protein that involves the combination of a colon-targeted peptide (TWYKIAFQRNRK, designated CT) with S100A8 and A9 peptide (Fig. 4a). CT peptide is specifically delivered to the colon as a carrier for colon delivery by binding to integrin α6β1, which is highly expressed in the colon as confirmed in our previous study [21]. The recombinant protein that we constructed was found to have no significant impact on cell viability (Fig. 4a). Second, the in vitro metabolic stability and pharmacokinetic parameters of rCT-S100A8/A9 were examined, and the results are summarized in Fig. 4b. rCT-S100A8/A9 exhibited excellent plasma and microsomal stability, with 100% and 92% remaining, respectively, after 30 min of treatment with rCT-S100A8/A9, PBS, human plasma, and human liver microsomes. Furthermore, the inhibitory activity of rCT-S100A8/A9 against the five most abundant CYP isozymes was evaluated to examine the toxicity of its drug–drug interaction. The results revealed that rCT-S100A8/A9 did not significantly decrease the activity of the tested CYP isozymes. Additionally, the S100A8/A9 peptide had similar effects. Third, the pharmacokinetic parameters of the intraperitoneally administered rCT-S100A8/A9 in female C57BL/6 mice were observed. The AUC value and half-life indicated that rCT-S100A8/A9 was well maintained in the blood at an effective drug concentration, which suggests that rCT-S100A8/A9, compared with the S100A8/A9 peptide, was suitable for in vivo experimentation. Overall, we confirmed that rCT-S100A8/A9 had appropriate drug-like properties, including in vitro stability and PK properties as well as pharmacological activity.

Fourth, we used a DSS-induced colitis mouse model to further investigate the physiological significance of rCT-S100A8/A9 in inflammatory colitis (Fig. S2). We found that the expression of ITGA6 (integrin α6) and ITGB1 (integrin β1), which bind to CT peptides, was substantially increased in the colon of mice with acute colitis (Fig. S2a). Next, we evaluated the specificity of rCT-S100A8/A9, and generated ITGA6- or ITGB1-knockdown mice through sh-lentiviral transduction. The mice were treated with DSS, and rCT-S100A8/A9-Cy5.5 was administered via intraperitoneal injection on day 6. The rCT, or rCT-S100A8/A9, specifically targeted the colonic tissues in mice with acute colitis but not the other organs, in a concentration-dependent manner (Figs. S2b and 2c). These results revealed that rCT binds to colonic tissues, which presented the possibility of designing a colon-targeted drug delivery system for use in pharmaceutical applications to treat DSS-induced colitis. Finally, we evaluated the pharmacodynamics of rCT-S100A8/A9, and FACS analysis showed that when rCT-S100A8/A9 was administered for three consecutive days in mice with acute DSS-induced colitis, 50% was retained in the colon (Fig. S2d).

Blockade of exogenous S100A8/A9 with rCT-S100A8/A9 ameliorates the progression of acute and chronic colitis

Next, we assessed the therapeutic efficacy of rCT-S100A8/A9 against DSS-induced acute colitis in mice. After inducing colitis with DSS, mice were intraperitoneally injected with rCT-S100A8/A9 (50 μg/kg) once a day for 6, 7, or 8 days, and sacrificed on day 12 to evaluate the effect of treatment frequency (Fig. 5a upper). The results showed that rCT-S100A8/A9 significantly increased the survival rates of mice with DSS-induced colitis in a treatment frequency-dependent manner (Fig. 5b bottom). Consistent with the pharmacological study (Fig. S2d), the group that received treatment for 3 consecutive days exhibited the highest survival rate. Furthermore, the rCT-S100A8/A9-treated groups exhibited reduced body weight loss and lower colitis scores than the control groups (rVehicle- or rCT-treated mice) (Fig. 5b). Next, we evaluated the length of the colon, an indicator of colitis. Colon length recovered in a manner proportional to the number of rCT-S100A8/A9 treatments (Fig. S3a). These changes were accompanied by increased hematoxylin and eosin (H&E) staining, suggesting that damage to the colon decreased with treatment frequency of rCT-S100A8/A9 (Fig. S3b).

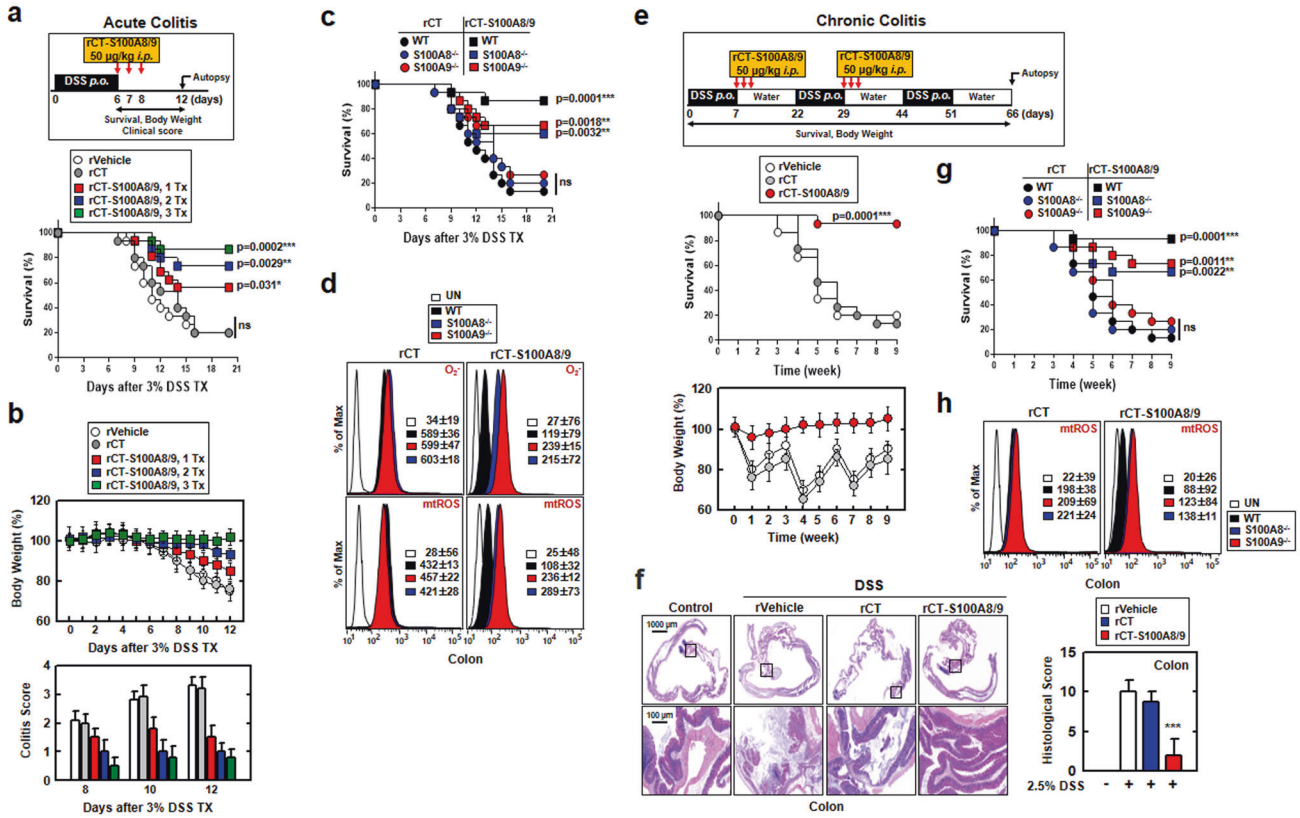

Fig. 5 rCT-S100A8/A9 has a therapeutic effect against DSS-induced acute and chronic colitis in mice. a Schematic of the acute colitis model treated 3% DSS with rCT-S100A8/9 (50 μg/kg) (upper). The survival of mice was monitored for 21 days; mortality was measured for $n = 15$ mice per group (lower). **b** Weight loss and colitis scores were obtained from clinical parameter (weight loss, stool consistency, bleeding) ($n = 10$). **c** The survival of S100A8$^{-/-}$, S100A8$^{-/-}$ compared to WT mice were monitored for 21 days ($n = 15$ mice per group). **d** FACS analysis for superoxide (up) and mitoROS (down). Quantitative analysis of mean fluorescence intensities of ROS (box). **e** Schematic of the chronic colitis model treated with 2.5% DSS and rCT-S100A8/9 (50 μg/kg) (upper). Middle, the survival of mice was monitored for 9 weeks; mortality was measured for $n = 15$ mice per group. Bottom, Weight loss of rVehicle, rCT or rCT-S100A8/9 in mice ($n = 15$). **f** Representative imaging of hematoxylin and eosin (H&E) staining of the colon (left) ($n = 10$). Histopathology scores were obtained from H&E staining as described in methods (Materials and Methods) were determined in 2.5% DSS-treated mice with rVehicle, rCT or rCT-S100A8/9 (right). **g** The survival of S100A8$^{-/-}$, S100A8$^{-/-}$ compared to WT mice were monitored for 9 weeks ($n = 15$ mice per group). **h** FACS analysis for mitoROS. Quantitative analysis of mean fluorescence intensities of ROS (box). Statistical differences compared with the rVehicle-treated mice (**a** and **e**) or rCT-treated mice (**c** and **g**) are indicated (log-rank test). The data are representative of two independent experiments with similar results (**a**, **c**, **e**, and **g**). Statistical significance was determined by Student's *t*-test with Bonferroni adjustment (***$P < 0.001$) compared with rVehicle (**f**).

To test whether rCT-S100A8/A9 exerted pharmacological activity in vivo, we analyzed the interactions of receptor-S100 and the activation of NLRP3 inflammasome in the colon of treatment and control groups. Upon DSS treatment, the interactions of TLR4 (or RAGE)-S100A8 (or S100A9) and NLRP3-ASC increased, but their interactions decreased following rCT-S100A8/A9 treatment, which also exhibited a trend depending on the frequency of administration (Fig. S3c). We also examined proinflammatory cytokine levels (TNF-α, IL-1β, IL-6, and IL-18) and the activity of myeloperoxidase (MPO) involved in the production of cytokines in colon homogenates (Fig. S3d). The results indicated that the levels of proinflammatory cytokines as well as MPO activity were significantly reduced in the colon homogenates of the mouse upon rCT-S100A8/A9 treatment. Notably, using experiments with S100A8 KO and S100A9 KO, rCT-S100A8/A9 was found to specifically regulate acute colitis survival (Fig. 5c) and ROS (cellular ROS and mtROS) (Fig. 5d) in S100A8 and S100A9-dependent manner.

We then confirmed the therapeutic effect of rCT-S100A8/A9 on chronic colitis. Chronic DSS colitis was induced by three cycles of DSS + water combinations and intraperitoneal rCT-S100A8/A9 injection was performed once a day for 3 consecutive days of DSS administration in each cycle. Similar to the acute colitis model, the rCT-S100A8/A9 group exhibited a pattern of significantly reduced body weight loss (Fig. 5e). Subsequently, we measured the length of the colon, which is an indication of colitis. Colon length recovered in the rCT-S100A8/A9-treated group (Fig. S3e). These changes were accompanied by increased hematoxylin and eosin (H&E) staining, suggesting decreased damage to the colon (Fig. 4f). Consistent with acute colitis, rCT-S100A8/A9 was found to specifically regulate chronic colitis survival (Fig. 5g) and ROS (Fig. 5h) in S100A8 and S100A9-dependent manner. However, macrophage polarization by rCT-S100A8/A9 was not affected in macrophages (Fig. S3f) and colon lysates (Fig. S3g).

The experimental results revealed that treatment with rCT-S100A8/A9 led to the reduction of acute and chronic inflammation in the colon through the blocking of TLR4 and RAGE, as well as regulation of the NLRP3 inflammasome. These findings underscore the necessity of further investigating rCT-S100A8/A9 as a candidate therapeutic agent for IBD.

rCT-S100A8/A9 attenuated tumorigenesis in CAC model

Growing evidence has suggested that chronic inflammation increases the risk of tumorigenesis. Therefore, we aimed to evaluate the therapeutic efficacy of rCT-S100A8/A9 to determine whether the progression of the "inflammation–cancer link" in a

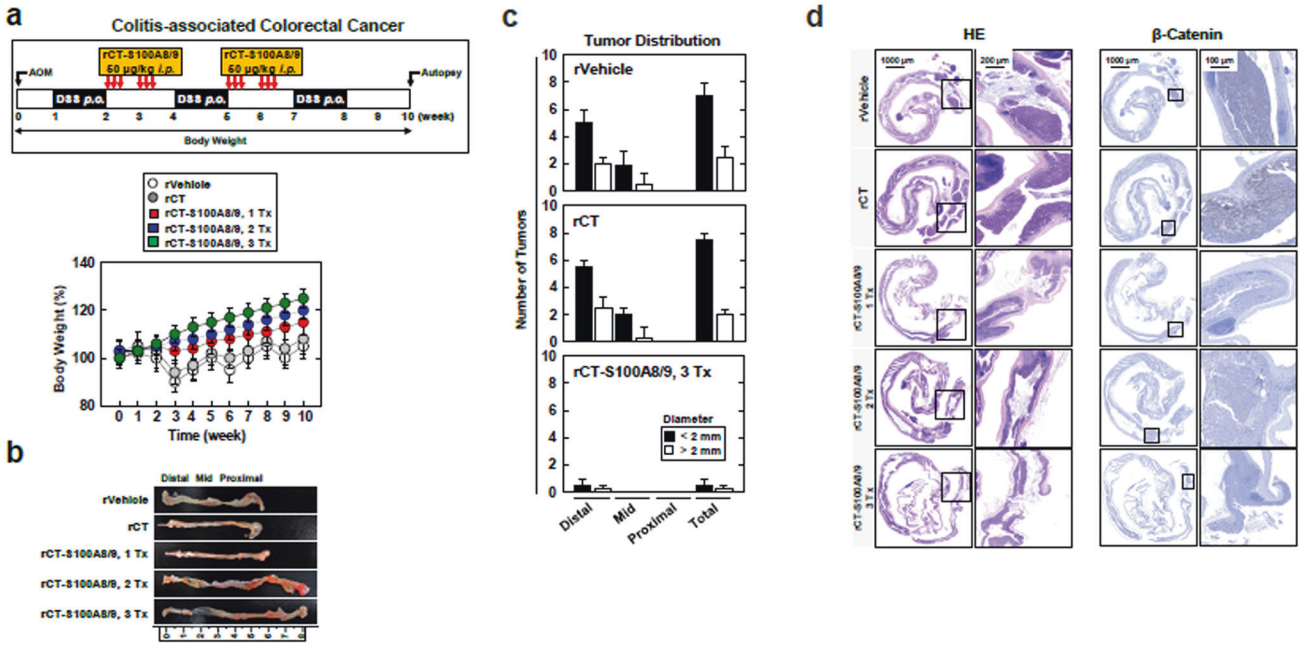

Fig. 6 rCT-S100A8/A9 has a therapeutic effect against AOM/DSS-induced colitis-associated colorectal cancer in mice. a Schematic of the AOM (10 mg/kg)/DSS (2.5%)-induced colitis-associated colorectal cancer model treated with rCT-S100A8/9 (50 μg/kg) (upper). Mouse weight relative to baseline during AOM/DSS administration. Weight loss in this experiment is a surrogate marker for colitis severity. The data are representative of two independent experiments with similar results. **b** Gross finding of the distal colon. Note the higher tumor burden in the distal colon/rectum and the characteristic rugated texture of the proximal colon with little tumor growth. **c** Representative distribution of the average number of tumors per mouse treated with AOM/DSS. Note the majority of tumors are located in the distal colon and are <2 mm in size. Data shown are the means ± SD of six experiments (**d**) Representative histology of a tumor resulting from AOM/DSS administration in the distal colon ($n = 10$). H&E and β-catenin stained slides demonstrate dysplastic changes similar to human adenocarcinomas of the colon.

CAC mouse model was suppressed by inhibiting the S100-PRRs interactions.

Mice treated with AOM/DSS received rCT-S100A8/A9 four times, depending on the administration frequency, during the administration of three DSS cycles until the 10th week (Fig. 6a, upper). The body weights of the CRC mice, treated with either rVehicle or rCT, showed a fluctuating trend with a lower increase in body weight, whereas treatment with rCT-S100A8/A9 resulted in a higher rate of body weight gain, which was more pronounced depending on the treatment frequency (Fig. 6a). The induction of tumors through AOM/DSS treatment was primarily observed in the distal colon and produced colon shortening in the CAC mouse model [35]. As illustrated in Fig. 6b, the control groups (rVehicle and rCT) displayed a high tumor burden in the distal colon, along with a shortened colon length. However, the colon length was restored in the rCT-S100A8/A9-treated groups, and the number of tumors <2 mm was significantly reduced in the group that received rCT-S100A8/A9 treatment for three consecutive days (Fig. 6c).

To further assess the colitis-associated tumors, H&E staining was performed. Histological analysis of the colon tissues obtained from the AOM/DSS-induced CRC mice revealed the presence of severe inflammation characterized by mucosal damage, superficial ulceration, and crypt epithelium destruction. However, the administration of rCT-S100A8/A9 demonstrated a significant alleviation of the histological colonic damage, specifically in terms of inflammatory infiltration and epithelial damage, as indicated by the preferential effects of the histological scores (Fig. 6d, left). Immunohistochemical analysis revealed the significant upregulation of β-catenin in the colon adenocarcinoma cells of CAC mice compared to the normal tissue; as expected (data not shown), treatment with rCT-S100A8/A9 effectively suppressed the protein levels of these markers (Fig. 6d, right). Furthermore, to determine the signaling mechanism and molecular target regulated by rCT-S100A8/A9, a profiler PCR array was performed on the CRC colon tissue, and it was confirmed that it regulates the involvement of the epithelial to mesenchymal transition (Fig. S4). Collectively, these observations indicate that rCT-S100A8/A9 treatment was effective in alleviating the progression of CAC.

rCT-S100A8/A9 inhibited oxaliplatin-resistant HCT116 xenograft tumor growth

Although oxaliplatin is an efficient chemotherapeutic commonly used for CRC treatment, its long-term use often leads to the development of drug resistance [24, 35]. Based on the evidence that rCT-S100A8/A9 alleviates colitis and CRC in a mouse model, we conducted experiments to investigate its efficacy in overcoming oxaliplatin resistance.

To test the inhibitory effect of rCT-S100A8/A9 on oxaliplatin resistance, we performed WST-8-based cell viability assays using three CRC cell lines, namely, parental HT29, HCT116, and SW480, as well as the corresponding oxaliplatin-resistant (OxaR) cell lines. OxaR CRC cells (HT29, HCT116, and SW480) were established through long-term exposure of CRC cells to oxaliplatin, as described in material and methods. As shown in Fig. 7a, OxaR CRC cells exhibited significant resistance to oxaliplatin treatment. rCT-S100A8/A9 treatment not only decreased the viability of OxaR CRC cells but also exhibited efficacy against multiple-drug resistance, including in doxorubicin-resistant (DoxR) and 5-fluorouracil-resistant (5-FuR) CRC cells (Fig. S5a).

Enhanced expression of TLR4 and RAGE on colon cancer cells following treatment with 5-FU and oxaliplatin was found to promote cell survival and induce epithelial–mesenchymal transition (EMT) through NF-κB signaling activation [36, 37]. Furthermore, extracellular binding of S100A8/A9 to these PRRs was found to lead to the activation of NF-κB, promoting tumor growth and chemoresistance [38, 39]. Therefore, we reasoned that the inhibitory effect of rCT-S100A8/A9 against OxaR CRC may stem from the blocking of S100-PRR interactions. In OxaR-HCT116, we

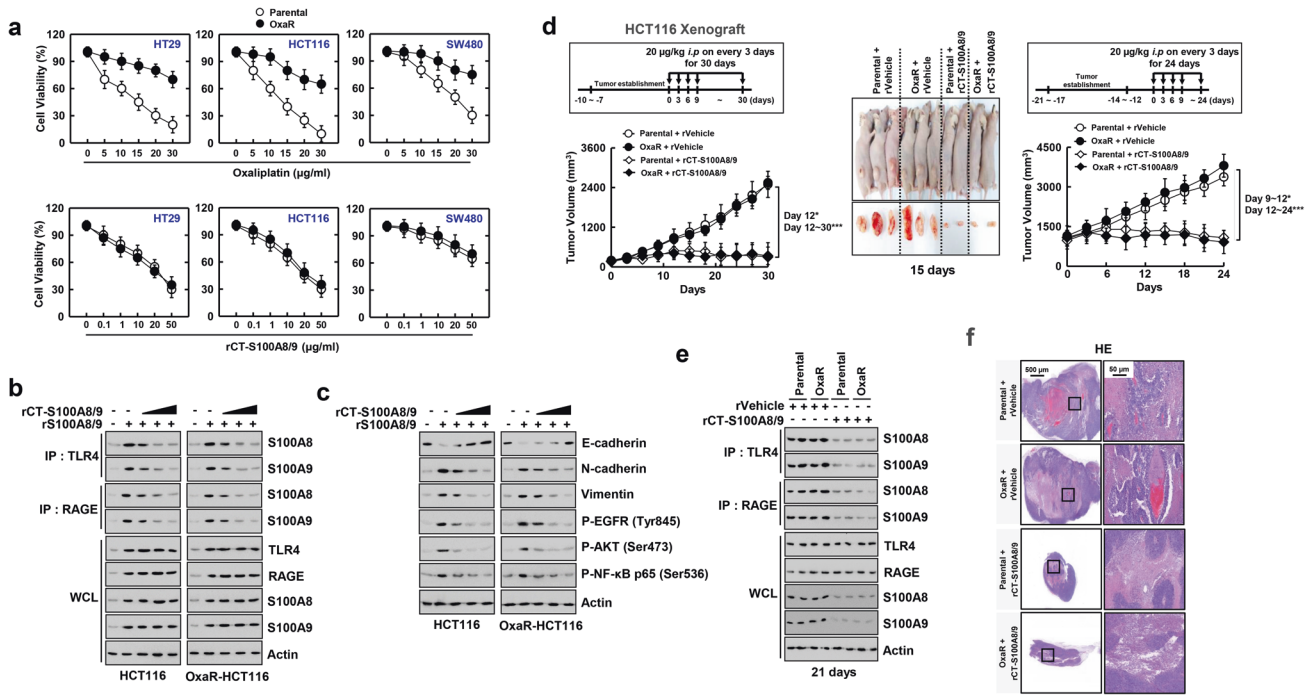

Fig. 7 rCT-S100A8/A9 ameliorated oxaliplatin-resistant HCT116 xenograft tumor growth. a Both parental and oxaliplatin-resistant HT29, HCT116, and SW480 colon cancer cell lines were treated with varying concentrations of oxaliplatin or rCT-S100A8/9 for 24 h and analyzed for cell viability. Each vertical bar shows the mean ± SD of cell viability in each dose. Data shown are the means ± SD of six experiments. **b**, **c** HCT116 of parental or OxaR were stimulated with rS100A8/9 (10 μg/ml) for 30 min, in presence of rCT-S100A8/9 (10, 20, 50 μg/ml) for 1 h. **b** HCT116 were subjected to IP with αTLR4 or αRAGE, followed by IB with αS100A8 or αS100A9. WCLs were used for IB with αTLR4, αRAGE, αS100A8, αS100A9 or αActin. **c** IB with αE-Cadherin, αN-Cadherin, αVimentin, αP-EGFR, αP-Akt, αP-NF-κB p65 or αActin. **d** Schematic of the xenograft model treated with rCT-S100A8/9 (upper). HCT116 cells were subcutaneously injected into the flanks of nude mice. The length and width of the tumors were measured using calipers, and the tumor volume was calculated every third day for 30 days. Representative images of tumors from mice treated with rCT-S100A8/9 on day 15 (Middle). Statistical significance was determined by two-way analysis of variance (ANOVA) with Tukey's post test; $^{*}P < 0.05$, $^{***}P < 0.001$ compared with rVehicle. **e** At day 21 after administration, the mice were euthanized, and tumor lysates were used for IP with αTLR4 or αRAGE, followed by IB with αS100A8 or αS100A9. WCLs were used for IB with αTLR4, αRAGE, αS100A8, αS100A9 or αActin. **f** Representative histology of a tumor ($n = 10$). H&E stained of the tumor. The data are representative of seven independent experiments with similar results (**b**, **c** and **e**).

observed that recombinant S100A8/A9 increased not only the expression of TLR4/RAGE, but also S100-PRR interactions, which was inhibited by an increasing concentration of rCT-S100A8/A9 (Fig. 7b). To confirm that the blocking of S100-PRR interactions correlates with the inhibitory effect on OxaR CRC, the cells treated with rCT-S100A8/A9 were lysed and subjected to Western blotting analysis to examine the expression of EMT markers. As shown in Fig. 7c, significantly reduced expression of mesenchymal markers (N-cadherin and Vimentin) and increased expression of an epithelial marker (E-cadherin) were observed in both parental and OxaR-HCT116 cells. Furthermore, the phosphorylation of EGFR, AKT, and NF-κB, involved in chemotherapy resistance pathways, was also reduced in both rCT-S100A8/A9-treated parental and OxaR CRC cells. These results suggest that targeting S100-PRR interactions by rCT-S100A8/A9 may be involved in the restoration of chemoresistance, thus exerting cytotoxic effects against OxaR CRC.

To assess the antitumor efficacy of rCT-S100A8/A9, we established xenograft mouse models using either parental or OxaR-HCT116 cells. When parental or OxaR-HCT116-bearing mice were intraperitoneally injected with rCT-S100A8/A9 at a dosage of 20 μg/kg, the presence of rCT-S100A8/A9 was detected in tumor cells by Western blot analysis. This localization of rCT-S100A8/A9 in tumor cells was observed to persist for up to 2 days after injection and had then diminished by the 3rd day (Fig. S5b).

Next, we performed tumor growth inhibition assays under various tumor growth conditions, initiating treatment with rCT-S100A8/A9 based on the size of the established tumors: starting rCT-S100A8/A9 treatment 10 days after tumor establishment for initial tumor growth, and starting rCT-S100A8/A9 treatment 21 days after tumor establishment for actively growing tumors. As expected, rCT-S100A8/A9 treatment significantly inhibited tumor growth in mice with both initially growing tumors and actively growing tumors (Fig. 7d). Western blotting showed that rCT-S100A8/A9 treatment significantly reduced the interaction of S100 with PRRs in xenograft tumors (Fig. 7e). Consistent with these findings (Fig. 7c), immunostaining of tumor sections using EMT markers showed increased expression of E-cadherin and decreased expression of N-cadherin and β-catenin in xenografts treated with rCT-S100A8/A9 compared with the levels in the control group.

The primary concern about protein therapeutics derived from endogenous human proteins is their potential to elicit a robust anti-therapeutic antibody response and to stimulate undesirable immune responses, which can include immune-mediated adverse effects and potential loss of efficacy [40]. We therefore assessed rCT-S100A8/A9's immunogenicity by measuring the generation of anti-rCT-S100A8/A9 antibodies in mice immunized with this peptide. There was negligible production of specific anti-rCT-S100A8/A9 antibodies, compared with that induced by ovalbumin (Fig. S5d). In addition, the production of proinflammatory cytokines induced by rCT-S100A8/A9 was negligible in mice with tumors. There were no differences in the serum levels of TNF-α, IL-6, and IL-1β between the negative control and rCT-S100A8/A9-administered mice (Fig. S5e), indicating that rCT-S100A8/A9 triggers insignificant immunogenicity and immune responses in

BALB/c mice. Furthermore, consistent with CRC, rCT-S100A8/A9 regulates the involvement of epithelial to mesenchymal transition on tumor of HCT116 xenografts by profiler PCR Array (Fig. S6).

Taking these findings together, rCT-S100A8/A9 efficiently increased the therapeutic effect of oxaliplatin-resistant CRC and is a biocompatible therapeutic candidate for which the issue of immunogenicity has been resolved.

DISCUSSION

The pronounced upregulation of S100A8 and S100A9 could be responsible for the aberrant activation of PRR signaling, which induces a vicious cycle of inflammatory responses and thus aggravates colon-associated disease [15, 41]. We found that serum S100A8 and S100A9 were elevated in acute and chronic DSS-induced colitis, and even in AOM/DSS-induced CRC models in mice, in which their interactions with their PRRs (TLR4 and RAGE) were significantly increased. Here, we prepared a platform of rCT-S100A8/A9 capable of targeting the colon and blocking S100(A8/A9)-PRR(TLR4/RAGE) interactions. rCT-S100A8/A9, conjugated with a colon-targeting peptide and TLR4/RAGE-inhibiting motifs derived from S100A8 and S100A9, successfully inhibited extracellular S100A8/A9-TLR4/RAGE interactions, thereby reducing colonic inflammation and disease severity in IBD-related mouse models including acute/chronic DSS-induced colitis mice and AOM/DSS-induced CRC mice. Furthermore, the therapeutic potential of targeting S100-PRR interactions using rCT-S100A8/A9 has been demonstrated in the context of OxaR xenografts. This approach has shown promise in reducing EMT-associated markers and tumor volume. Taken together, our findings establish a proof of concept for targeting S100-PRR interactions as a strategy to prevent chronic intestinal inflammation, with potential relevance for both IBD and CRC.

TLR4 and RAGE, as crucial innate immune sensors, are indeed expressed on various cells, including immune cells and cancer cells. These PRRs have already been implicated in sterile inflammation in the absence of any microbial ligands [42]. The dysregulation of these PRRs has been associated with poor prognosis in various diseases, including infectious diseases, chronic inflammatory conditions, and certain types of cancers. Under inflammatory conditions, their expression and activation by DAMPs are often upregulated, which enhances immune cell activation and the production of proinflammatory cytokines. In the tumor microenvironment, S100A8 and S100A9 can stimulate TLR4/RAGE signaling in cancer, which promotes tumor cell proliferation, survival, invasion, angiogenesis, and immune evasion [43]. Notably, it has been shown that the expression levels of TLR4 and RAGE are increased in colonocytes and the lamina propria in patients with active ulcerative colitis [44, 45]. Thus, targeting the S100A8/A9-TLR4/RAGE axis may provide a therapeutic benefit for developing broad-spectrum anti-inflammatory and anti-cancer therapies. Therapeutics peptides targeting macrophages have several advantages, including economic benefits, feasibility of clinical-grade manufacturing, and applicability to inflammatory diseases therapy. By determining the impact of peptide length and formulation on their immunogenicity, we showed that peptide-based agents can be used and lead to major breakthroughs. However, S100A8 and S100A9 are widely overexpressed in many inflammations like infection-induced inflammations and metabolic inflammations, and the normal expression of those proteins was proved to be functional for many intracellular and extracellular processes, maybe has the potential risks of rCT-S100A8. Thus, challenges remain in large-scale synthesis, safe delivery, and efficient immunotherapy to improve next-generation peptide-based immunotherapy.

Abnormal activation of the NLRP3 inflammasome has been detected in inflamed tissues of murine models and patients with IBD, indicating its potential pathogenic involvement in the disease [46]. TLR4 and RAGE have been found to be strongly associated with colonic inflammation via their involvement in the assembly of the PYD, LRR, and NACHT domains of the NLRP3 inflammasome by the activating NF-κB pathway. This subsequently leads to the expression of NLRP3 and IL-1β [47]. In LPS-primed BMDMs, our S100A8/A9 peptide effectively inhibited the interactions between NLRP3 and ASC, indicating its involvement in regulating the activation process. We found that rCT-S100A8/A9 could inhibit the pathogenesis of colitis and CRC by modulating activation of the NLRP3 inflammasome. Our study using DSS-induced colitis models indicated that rCT-S100A8/A9 successfully reduced the secretion of IL-1β and IL-18, which was also associated with the inhibition of NLRP3-ASC interactions. The ability of rCT-S100A8/A9 to modulate the activation of NLRP3 inflammasome suggests its potential for disrupting the inflammatory feedback loop resulting from excessive TLR4/RAGE responses and re-establishing a physiologically appropriate immune response in colonic diseases. However, further research is needed to investigate the specific mechanisms by which rCT-S100A8/A9 regulates the NLRP3 inflammasome, including whether it works indirectly through blocking TLR4/RAGE signaling or through other unknown mechanisms.

Macrophages are now increasingly acknowledged as crucial contributors to the maintenance of intestinal homeostasis and serve as important sentinels of the intestinal immune system. The well-balanced differentiation and activation of macrophage subsets are critical factors in achieving these functions, as they contribute to the overall health and functionality of the colonic immune system. Recently, it has been reported that the overexpression of S100A9 in obesity disrupts the development of M2-like macrophages through TLR4-NFκB signaling. This in turn results in the induction of TLR4-dependent IL-1β release by S100A9 in macrophages, which exacerbates skin inflammation and impairs wound healing [48]. Indeed, S100A9 has been shown to regulate the immunosuppression mediated by myeloid-derived suppressor cells (MDSCs) in colorectal carcinoma in a manner involving the RAGE and TLR4 signaling pathways [49]. The immunosuppressive activity of MDSC-derived macrophages is dependent on the persistent expression of S100A9 protein in these cells. S100A9 also promotes the M2 polarization of macrophages [50]. This highlights the role of S100A9 in modulating macrophage plasticity and function in response to specific disease conditions, underscoring its significance in shaping the immune response and inflammation-associated with those diseases. Given that TLR4/RAGE expression in macrophages is highly upregulated in inflamed colon, it is reasonable to assume that targeting S100-PRR interactions has the potential to regulate macrophage polarization toward a balanced phenotype in the context of intestinal inflammation. We further demonstrated that rCT-S100A8/A9 reduced NLRP3 inflammasome-mediated release of IL-1β.

TLR4- and RAGE-targeted therapies are currently under development for acute and chronic inflammation. While they hold promise, some potential side effects associated with these inhibitors include increased susceptibility to infection [51] and impaired wound healing [52]. This is understandable as these PRRs play crucial roles in recognizing and responding to microbial pathogens. Therefore, when considering therapeutic interventions targeting TLR4 and RAGE, it is crucial to carefully balance the potential benefits with the potential risks and to develop strategies that selectively modulate their activity rather than eliminate it. In terms of therapy, targeting the S100/TLR4/RAGE axis instead of directly targeting the PRRs themselves offers a clear advantage. By specifically blocking the interactions between S100 proteins and TLR4/RAGE, the focus is on disrupting the detrimental effects associated with the axis while potentially preserving the TLR4-dependent antimicrobial defense mechanisms. Thus, disrupting the inflammatory feedback loop resulting from excessive TLR4/RAGE responses by S100A8/A9 would curtail

inflammation and restore a physiologically appropriate immune response to pathogens, preventing the excessive production of proinflammatory cytokines and chemokines.

In conclusion, we showed that the treatment of mice with rCT-S100A8/A9 during acute/chronic colitis and colitis-associated CRC development had a protective effect against intestinal inflammation and tumorigenesis. This suggests that blocking S100-PRR interactions is a potential therapeutic target for inflammation-associated colonic diseases. Our study introduces a proof of concept for utilizing dual PRR-inhibiting systems to prevent chronic intestinal inflammation, which has potential applications in both IBD and CRC.

ACKNOWLEDGEMENTS

We would like to thank all members of the Infection Biology Lab for critical reading and discussion of the manuscript. This work was supported by a National Research Foundation of Korea grant funded by the Korea government (MSIP) (grant no. 2019R1I1A2A01064237 and 2021R1A4A5032463), by a grant of the Korea Health Technology R&D Project through the Korea Health Industry Development Institute (KHIDI), funded by the Ministry of Health &Welfare, Republic of Korea (HI22C0884). EC was supported by the Health Fellowship Foundation.

AUTHOR CONTRIBUTIONS

EC, SJM, HKK, YSH, and WJG performed molecular and animal experiments and also analyzed the data. CSY designed and conceptualized the research supervised the experimental work, analyzed the data, and wrote the manuscript

ADDITIONAL INFORMATION

Supplementary information The online version contains supplementary material available at https://doi.org/10.1038/s41401-023-01188-2.

Competing interests: The authors declare no competing interests.

REFERENCES

1. Neurath MF. Targeting immune cell circuits and trafficking in inflammatory bowel disease. Nat Immunol. 2019;20:970–9.
2. Vuyyuru SK, Kedia S, Sahu P, Ahuja V. Immune-mediated inflammatory diseases of the gastrointestinal tract: beyond Crohn's disease and ulcerative colitis. JGH Open. 2022;6:100–11.
3. Kim ER, Chang DK. Colorectal cancer in inflammatory bowel disease: the risk, pathogenesis, prevention and diagnosis. World J Gastroenterol. 2014;20:9872–81.
4. Eaden JA, Abrams KR, Mayberry JF. The risk of colorectal cancer in ulcerative colitis: a meta-analysis. Gut. 2001;48:526–35.
5. Danese S, Vuitton L, Peyrin-Biroulet L. Biologic agents for IBD: practical insights. Nat Rev Gastroenterol Hepatol. 2015;12:537–45.
6. Gaujoux R, Starosvetsky E, Maimon N, Vallania F, Bar-Yoseph H, Pressman S, et al. Cell-centred meta-analysis reveals baseline predictors of anti-TNFalpha non-response in biopsy and blood of patients with IBD. Gut. 2019;68:604–14.
7. Nixon AB, Sibley AB, Liu Y, Hatch AJ, Jiang C, Mulkey F, et al. Plasma protein biomarkers in advanced or metastatic colorectal cancer patients receiving chemotherapy with bevacizumab or cetuximab: results from CALGB 80405 (Alliance). Clin Cancer Res. 2022;28:2779–88.
8. Krasteva N, Georgieva M. Promising therapeutic strategies for colorectal cancer treatment based on nanomaterials. Pharmaceutics. 2022;14:1213.
9. Miller KD, Nogueira L, Mariotto AB, Rowland JH, Yabroff KR, Alfano CM, et al. Cancer treatment and survivorship statistics, 2019. CA Cancer J Clin. 2019;69:363–85.
10. Xie YH, Chen YX, Fang JY. Comprehensive review of targeted therapy for colorectal cancer. Signal Transduct Target Ther. 2020;5:22.
11. Ma L, Sun P, Zhang JC, Zhang Q, Yao SL. Proinflammatory effects of S100A8/A9 via TLR4 and RAGE signaling pathways in BV-2 microglial cells. Int J Mol Med. 2017;40:31–8.
12. Chakraborty D, Zenker S, Rossaint J, Holscher A, Pohlen M, Zarbock A, et al. Alarmin S100A8 activates alveolar epithelial cells in the context of acute lung injury in a TLR4-dependent manner. Front Immunol. 2017;8:1493.
13. Meuwis MA, Vernier-Massouille G, Grimaud JC, Bouhnik Y, Laharie D, Piver E, et al. Serum calprotectin as a biomarker for Crohn's disease. J Crohns Colitis. 2013;7:e678–83.
14. Pepper RJ, Hamour S, Chavele KM, Todd SK, Rasmussen N, Flint S, et al. Leukocyte and serum S100A8/S100A9 expression reflects disease activity in ANCA-associated vasculitis and glomerulonephritis. Kidney Int. 2013;83:1150–8.
15. Boyapati RK, Rossi AG, Satsangi J, Ho GT. Gut mucosal DAMPs in IBD: from mechanisms to therapeutic implications. Mucosal Immunol. 2016;9:567–82.
16. Benoit S, Toksoy A, Ahlmann M, Schmidt M, Sunderkotter C, Foell D, et al. Elevated serum levels of calcium-binding S100 proteins A8 and A9 reflect disease activity and abnormal differentiation of keratinocytes in psoriasis. Br J Dermatol. 2006;155:62–6.
17. Shi C, Dawulieti J, Shi F, Yang C, Qin Q, Shi T, et al. A nanoparticulate dual scavenger for targeted therapy of inflammatory bowel disease. Sci Adv. 2022;8:eabj2372.
18. Arevalo-Perez R, Maderuelo C, Lanao JM. Recent advances in colon drug delivery systems. J Control Release. 2020;327:703–24.
19. Kumar R, Islam T, Nurunnabi M. Mucoadhesive carriers for oral drug delivery. J Control Release. 2022;351:504–59.
20. Ren Y, Mu Y, Song Y, Xie J, Yu H, Gao S, et al. A new peptide ligand for colon cancer targeted delivery of micelles. Drug Deliv. 2016;23:1763–72.
21. Kim JS, Kim HK, Kim M, Jang S, Cho E, Mun SJ, et al. Colon-Targeted eNAMPT-Specific Peptide Systems for Treatment of DSS-Induced Acute and Chronic Colitis in Mouse. Antioxidants. 2022;11:2376.
22. Kim JS, Kim HK, Lee J, Jang S, Cho E, Mun SJ, et al. Inhibition of CD82 improves colitis by increasing NLRP3 deubiquitination by BRCC3. Cell Mol Immunol. 2023;20:189–200.
23. Hsu HH, Chen MC, Baskaran R, Lin YM, Day CH, Lin YJ, et al. Oxaliplatin resistance in colorectal cancer cells is mediated via activation of ABCG2 to alleviate ER stress induced apoptosis. J Cell Physiol. 2018;233:5458–67.
24. Sun W, Ge Y, Cui J, Yu Y, Liu B. Scutellarin resensitizes oxaliplatin-resistant colorectal cancer cells to oxaliplatin treatment through inhibition of PKM2. Mol Ther Oncolytics. 2021;21:87–97.
25. Greenlee JD, Lopez-Cavestany M, Ortiz-Otero N, Liu K, Subramanian T, Cagir B, et al. Oxaliplatin resistance in colorectal cancer enhances TRAIL sensitivity via death receptor 4 upregulation and lipid raft localization. eLife. 2021;10:e67750.
26. Duan L, Wu R, Ye L, Wang H, Yang X, Zhang Y, et al. S100A8 and S100A9 are associated with colorectal carcinoma progression and contribute to colorectal carcinoma cell survival and migration via Wnt/beta-catenin pathway. PLoS One. 2013;8:e62092.
27. Pu W, Zhang H, Zhang T, Guo X, Wang X, Tang S. Inhibitory effects of *Clostridium butyricum* culture and supernatant on inflammatory colorectal cancer in mice. Front Immunol. 2023;14:1004756.
28. Baroja-Mazo A, Martin-Sanchez F, Gomez AI, Martinez CM, Amores-Iniesta J, Compan V, et al. The NLRP3 inflammasome is released as a particulate danger signal that amplifies the inflammatory response. Nat Immunol. 2014;15:738–48.
29. Roh JS, Sohn DH. Damage-associated molecular patterns in inflammatory diseases. Immune Netw. 2018;18:e27.
30. Bresnick AR, Weber DJ, Zimmer DB. S100 proteins in cancer. Nat Rev Cancer. 2015;15:96–109.
31. Singh P, Ali SA. Multifunctional role of S100 protein family in the immune system: an update. Cells. 2022;11:2274.
32. Chen QL, Yin HR, He QY, Wang Y. Targeting the NLRP3 inflammasome as new therapeutic avenue for inflammatory bowel disease. Biomed Pharmacother. 2021;138:111442.
33. Bai B, Yang Y, Wang Q, Li M, Tian C, Liu Y, et al. NLRP3 inflammasome in endothelial dysfunction. Cell Death Dis. 2020;11:776.
34. Bauer C, Duewell P, Mayer C, Lehr HA, Fitzgerald KA, Dauer M, et al. Colitis induced in mice with dextran sulfate sodium (DSS) is mediated by the NLRP3 inflammasome. Gut. 2010;59:1192–9.
35. Wang H, Wang X, Zhang H, Deng T, Liu R, Liu Y, et al. The HSF1/miR-135b-5p axis induces protective autophagy to promote oxaliplatin resistance through the MUL1/ULK1 pathway in colorectal cancer. Oncogene. 2021;40:4695–708.
36. Kim YHCAD. Enhanced TLR4 expression on colon cancer cells after chemotherapy promotes cell survival and epithelial–mesenchymal transition through phosphorylation of GSK3β. Anticancer Res. 2016;36:3383–94.
37. Santaolalla R, Sussman DA, Ruiz JR, Davies JM, Pastorini C, Espana CL, et al. TLR4 activates the beta-catenin pathway to cause intestinal neoplasia. PLoS One. 2013;8:e63298.
38. Turovskaya O, Foell D, Sinha P, Vogl T, Newlin R, Nayak J, et al. RAGE, carboxylated glycans, and S100A8/A9 play essential roles in colitis-associated carcinogenesis. Carcinogenesis. 2008;29:2035–43.
39. Ichikawa M, Williams R, Wang L, Vogl T, Srikrishna G. S100A8/A9 activate key genes and pathways in colon tumor progression. Mol Cancer Res. 2011;9:133–48.
40. Baker MP, Reynolds HM, Lumicisi B, Bryson CJ. Immunogenicity of protein therapeutics: the key causes, consequences and challenges. Self Nonself. 2010;1:314–22.

41. Guo Q, Zhao Y, Li J, Liu J, Yang X, Guo X, et al. Induction of alarmin S100A8/A9 mediates activation of aberrant neutrophils in the pathogenesis of COVID-19. Cell Host Microbe. 2021;29:222–35.
42. Vogl T, Stratis A, Wixler V, Voller T, Thurainayagam S, Jorch SK, et al. Auto-inhibitory regulation of S100A8/S100A9 alarmin activity locally restricts sterile inflammation. J Clin Invest. 2018;128:1852–66.
43. Jang GY, Lee JW, Kim YS, Lee SE, Han HD, Hong KJ, et al. Interactions between tumor-derived proteins and Toll-like receptors. Exp Mol Med. 2020;52:1926–35.
44. Ungaro R, Mehandru S, Allen PB, Peyrin-Biroulet L, Colombel JF. Ulcerative colitis. Lancet. 2017;389:1756–70.
45. Body-Malapel M, Djouina M, Waxin C, Langlois A, Gower-Rousseau C, Zerbib P, et al. The RAGE signaling pathway is involved in intestinal inflammation and represents a promising therapeutic target for inflammatory bowel diseases. Mucosal Immunol. 2019;12:468–78.
46. Tourkochristou E, Aggeletopoulou I, Konstantakis C, Triantos C. Role of NLRP3 inflammasome in inflammatory bowel diseases. World J Gastroenterol. 2019;25:4796–804.
47. Yang Y, Wang H, Kouadir M, Song H, Shi F. Recent advances in the mechanisms of NLRP3 inflammasome activation and its inhibitors. Cell Death Dis. 2019;10:128.
48. Franz S, Ertel A, Engel KM, Simon JC, Saalbach A. Overexpression of S100A9 in obesity impairs macrophage differentiation via TLR4-NF-κB-signaling worsening inflammation and wound healing. Theranostics. 2022;12:1659–82.
49. Huang M, Wu R, Chen L, Peng Q, Li S, Zhang Y, et al. S100A9 regulates MDSCs-mediated immune suppression via the RAGE and TLR4 signaling pathways in colorectal carcinoma. Front Immunol. 2019;10:2243.
50. Kwak T, Wang F, Deng H, Condamine T, Kumar V, Perego M, et al. Distinct populations of immune-suppressive macrophages differentiate from monocytic myeloid-derived suppressor cells in cancer. Cell Rep. 2020;33:108571.
51. Haastrup PF, Thompson W, Sondergaard J, Jarbol DE. Side effects of long-term proton pump inhibitor use: a review. Basic Clin Pharmacol Toxicol. 2018;123:114–21.
52. Stuermer EK, Besser M, Terberger N, Bachmann HS, Severing AL. Side effects of frequently used antihypertensive drugs on wound healing in vitro. Ski Pharm Physiol. 2019;32:162–72.